THE JOURNAL OF PHYSICAL CHEMISTRY A
A JOURNAL OF THE AMERICAN CHEMICAL SOCIETY

pubs.acs.org/JPCA

Article

Dissociative Photoionization of Methyl Vinyl Ketone−Thermochemical Anchors and a Drifting Methyl Group

Published as part of The Journal of Physical Chemistry virtual special issue "Cheuk-Yiu Ng Festschrift".

Peter Weidner, Amelia W. Ray, Andras Bodi, and Bálint Sztáray*

Cite This: *J. Phys. Chem. A* 2021, 125, 848−856

Read Online

ACCESS | Metrics & More | Article Recommendations

ABSTRACT: The dissociative photoionization of methyl vinyl ketone (MVK), an important intermediate in the atmospheric oxidation of isoprene, has been studied by photoelectron photoion coincidence spectroscopy. In the photon energy range of 9.5−13.8 eV, four main fragment ions were detected at m/z 55, 43, 42, and 27 aside from the parent ion at m/z 70. The m/z 55 fragment ion ($C_2H_3CO^+$) is formed from ionized MVK by direct methyl loss, while breaking the C−C bond on the other side of the carbonyl group results in the acetyl cation (CH_3CO^+, m/z 43) and the vinyl radical. The m/z 42 fragment ion is formed via a CO-loss from the molecular ion after a methyl shift. The lightest fragment ion, the vinyl cation ($C_2H_3^+$ at m/z 27), is produced in two different reactions: acetyl radical loss from the molecular ion and CO-loss from $C_2H_3CO^+$. Their contributions to the m/z 27 signal are quantified based on the acetyl and vinyl fragment thermochemical anchors and quantum chemical calculations. Based on the experimentally derived appearance energy of the m/z 43 fragment ion, a new, experimentally derived heat of formation is proposed herein for gaseous methyl vinyl ketone ($\Delta_f H_{0K}$ = −94.3 ± 4.8 kJ mol^{-1}; $\Delta_f H_{298K}$ = −110.5 ± 4.8 kJ mol^{-1}), together with cationic heats of formation and bond dissociation energies.

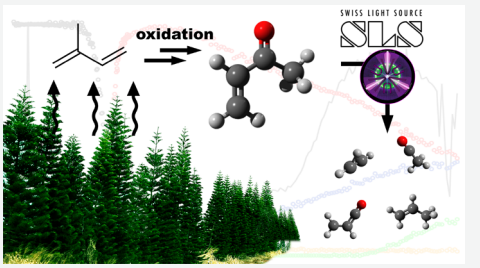

INTRODUCTION

Naturally occurring volatile organic compounds from biogenic sources play an important role in atmospheric photochemistry. The most abundant of these compounds is isoprene, which is produced at an estimated rate of 500 Tg year^{-1}, accounting for approximately half of the annual biogenic non-methane hydrocarbon emission worldwide.[1−3] Isoprene readily undergoes oxidation in the atmosphere and one of its main oxidation intermediates is methyl vinyl ketone. As isoprene shows high reactivity toward numerous oxidizers, it has a major influence on atmospheric oxidation chemistry by impacting the radical pool.[4−6] In a recent review, Wennberg *et al.* give an extensive summary of these reactions,[7] outlining the complexity of atmospheric isoprene oxidation. Although atmospheric reactions of isoprene have been well studied,[7,8] there is less information on the gas-phase chemistry of the main oxidation intermediates, *e.g.*, methyl vinyl ketone, methacrolein, allyl methyl ketone, methylglyoxal, glyoxal, and hydroxyacetone.

In addition to being one of the main oxidation intermediates of isoprene, methyl vinyl ketone (MVK) is the simplest unsaturated ketone and a model compound for more complex ketones. Available literature on the gas-phase chemistry of methyl vinyl ketone focuses mostly on photolysis and photooxidation,[9−14] but the reported dissociation reactions in the neutral are remarkably similar to the ionic dissociation processes of MVK (*vide infra*). On the one hand, Fahr *et al.* studied the photolysis of neutral methyl vinyl ketone at 193 nm.[10] They found that the two main radical products of this process are methyl and vinyl radicals, which are proposed to form as $CH_3COC_2H_3 \rightarrow CH_3 + C_2H_3 + CO$. On the other hand, lower energy photolysis at 308 nm of neutral MVK is dominated not by radicals but by the molecular products propene and carbon monoxide as shown by Earle *et al.*[9] Formation of MVK through the OH-initiated oxidation of isoprene and further oxidation of the title compound was studied by Pan *et al.*, utilizing photoionization mass spectrometry (PIMS) with synchrotron vacuum ultraviolet radiation.[12] They reported the adiabatic ionization energy of MVK as 9.66 eV.

In this work, MVK has been studied by photoelectron photoion coincidence (PEPICO) spectroscopy, which provides complementary data to the literature on the gas-phase chemistry of MVK, especially when it comes to thermochemistry. Our project also serves as a logical continuation of experimental studies on small oxygenated species with atmospheric or combustion relevance. Threshold PEPICO

Received: November 27, 2020
Revised: December 29, 2020
Published: January 19, 2021

https://dx.doi.org/10.1021/acs.jpca.0c10665
J. Phys. Chem. A 2021, 125, 848−856

(TPEPICO) experiments on the simplest ketone, acetone, unveiled its dissociative photoionization mechanism as well as thermochemical data of both the neutral molecule and its fragments.[15−17] In a recent study on isopropanol,[18] we discussed direct and roaming H-abstraction pathways, which are important in the dissociative photoionization of methyl hydroperoxide[19] and acetone,[20] as well as in the structurally similar urea[21] and acetamide.[22] Hydrogen scrambling plays a subordinate role in the dissociative photoionization of longer chain species, *e.g.*, butanone, the second simplest acyclic ketone, which was investigated by TPEPICO spectroscopy by Kercher *et al.*[23] Instead, the main dissociation reactions close to the butanone ionization energy are methyl and ethyl radical losses, corresponding to C−C bond cleavages on either side of the carbonyl group. Acrolein shows a high degree of structural similarity to MVK and its dissociative photoionization was studied by Li and Baer.[24] The lowest-energy channel in the dissociation of the acrolein ion corresponds to CO-loss. This reaction proceeds through a tight transition state, therefore, it is overcome by H-loss from the aldehyde group at higher energies. As we will discuss, MVK cations exhibit similar dissociation reactions to these carbonyl systems, including direct single bond cleavage reactions and also rearrangement-initiated CO-loss.

PEPICO experiments provide accurate thermochemical data for molecules, radicals, and ions.[25−30] Despite the importance of methyl vinyl ketone as a key intermediate in the atmospheric oxidation of isoprene, only a tentative gas-phase heat of formation is available in the literature, based on the cross-hydrogenation equilibrium with 2-ethyl-2-methyl-1,3-dioxolane in benzene.[31] The most commonly used values are based on empirical rules or quantum chemical calculations (*vide infra*). In addition to examining the dissociative photoionization mechanism of MVK, we also aim to provide accurate, new and/or updated thermochemical data on the neutral precursor molecule, its molecular ion, and some of the fragment ions. These gas-phase energetics data are useful in modeling reaction systems, which are hard to study directly, *e.g.*, in atmospheric, combustion, or even extraterrestrial environments.

MATERIALS AND METHODS

Experiment. Methyl vinyl ketone (≥99% purity) was purchased from Sigma−Aldrich and used without further purification. Gas-phase MVK was sampled from the headspace of a room temperature glass vial and introduced via an effusive inlet into the ionization chamber of the CRF-PEPICO (Combustion Reactions Followed by PEPICO) endstation of the vacuum ultraviolet (VUV) beamline at the Swiss Light Source.[32] The instrument has been described in detail previously[33] and only the relevant parts of the experimental setup are discussed here.

Prior to interaction with the sample, VUV synchrotron radiation was collimated, dispersed in grazing incidence by a 600 grooves/mm laminar grating, and focused at the exit slit in a differentially pumped gas filter at a resolution of better than 5 meV. Higher harmonics were suppressed by a factor of more than 10^6 by a Ne−Ar−Kr mixture at 10 mbar pressure over 10 cm optical length. The photon energy was calibrated using Ar and Ne 11s′−14s′ autoionization lines in first and second orders of the grating. The pressure in the experimental chamber was kept at ∼9×10^{-7} mbar during the experiment.

The effusively introduced, room temperature sample was intersected by tunable synchrotron VUV light in an approximately 2 × 2 mm cross-section interaction region. The resulting photoelectrons and photoions were extracted from the ionization region, accelerated toward opposite ends of the experimental setup by a 125 V cm^{-1} electric field, and detected in delayed coincidence using a multiple-start/multiple-stop coincidence acquisition scheme.[34] The start signal for coincidence analysis is provided by the photoelectrons. They are kinetic energy analyzed by velocity map imaging (VMI)[35] on a Roentdek DLD40 position sensitive delay line detector mounted 750 mm from the ionization point with sub-meV resolution at threshold. Zero kinetic energy (threshold) electrons and energetic ("hot") electrons with no off-axis momentum are both detected in the center of the image. The hot electron contamination in the center photoelectron signal was corrected by subtracting coincidence events corresponding to a ring area around the detector center, multiplied by an experimentally determined factor (approximately the area ratio of these regions of interest). The corresponding photoions, used as a stop signal in the coincidence acquisition scheme, were mass analyzed using a two-stage Wiley−McLaren TOF mass spectrometer[36] with a 2.7 cm long extraction, an 8.7 cm long acceleration, and an 88.6 cm long field-free drift region and detected by a Roentdek DLD40 microchannel plate detector. The 125 V cm^{-1} extraction field and the long extraction region lead to ion residence times in the order of microseconds. Consequently, metastable parent ions with unimolecular reaction rates between 10^3 and 10^7 s^{-1} yield asymmetric peaks in the time-of-flight coincidence spectra. Fractional abundances of ions detected in coincidence with threshold electrons were plotted as a function of photon energy to obtain the breakdown diagram (Figure 1) while the threshold photoelectron spectrum (TPES), also depicted in Figure 1, is obtained by plotting the threshold electron count rate as a function of photon energy.

Computation. The Gaussian 09 suite of programs[37] was used to carry out *ab initio* quantum chemical calculations to find the dissociative photoionization reaction pathways of methyl vinyl ketone. Minimum structures were first optimized at the B3LYP/6-311++G(d,p) level,[38,39] providing initial input for the statistical modeling. Reaction pathways and transition

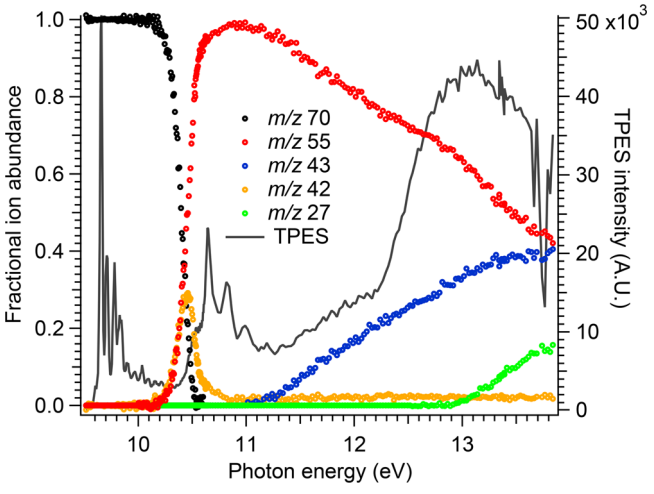

Figure 1. Experimental breakdown diagram (open circles) and the experimentally measured threshold photoelectron spectrum (solid black line) of methyl vinyl ketone.

https://dx.doi.org/10.1021/acs.jpca.0c10665
J. Phys. Chem. A 2021, 125, 848−856

state (TS) structures were located by constrained optimizations and reaction coordinate scans. Transition-state structures were verified by intrinsic reaction coordinate (IRC) calculations.[40] Finally, energies of the stationary points on the potential energy surface that most likely play a part in the dissociative photoionization of methyl vinyl ketone were refined using the G4 and W1U methods.[41−43]

Statistical Modeling. Our modeling approach is described in detail elsewhere,[44] and only the topical aspects are discussed here. Two approaches were used to calculate the microcanonical unimolecular rate constants $k(E)$ for each dissociation channel: the rigid activated complex (rac-)Rice−Ramsperger−Kassel−Marcus (RRKM)[45−47] and the simplified statistical adiabatic channel (SSACM) theories.[44] In both cases, the internal-energy dependent unimolecular rate constants are obtained based on the following equation:

$$k(E) = \frac{\sigma N^{\ddagger}(E - E_0)}{h\rho(E)}$$

$N^{\ddagger}(E - E_0)$ is the number of states of the transition state at given excess energy (E) above the threshold at E_0, $\rho(E)$ is the density of states of the molecule, h is Planck's constant, and σ is the symmetry number of the reaction. The Beyer−Swinehart direct count algorithm[48] was used to calculate densities and sums of states from the harmonic vibrational frequencies.

The two approaches mainly differ by how they treat the transition state model and calculate $N^{\ddagger}(E - E_0)$. In rac-RRKM theory, the number of states function is calculated at the transition state geometry, which corresponds to a saddle point on the potential energy surface. Alternatively, the frequencies can be evaluated at an arbitrarily chosen geometry along the reaction coordinate if it is monotonically attractive. SSACM, an extension to the phase space theory (PST), considers the product degrees of freedom when calculating the bottleneck along the potential energy surface. To calculate $N^{\ddagger}(E - E_0)$, an energy dependent rigidity factor is used in concert with the product number of states to account for the anisotropy of the potential energy surface. Although rac-RRKM usually provides a reliable estimate for the kinetic and competitive shift in most cases and has been extensively used to model PEPICO data, we have shown that it tends to overestimate kinetic and competitive shifts for fragmentations without a reverse barrier, especially if they are considerable, and underestimates the E_0.[49,50] In such cases, SSACM extrapolates to the distant E_0 value more accurately. However, it underperforms when modeling reactions involving constrained transition state structures and is prone to yield unphysical rate curves or even dropping rates with energy at high internal energies.[44] Based on the work of Chupka,[51] Lifshitz defines a kinetic shift as "the excess energy required to produce detectable dissociation of a polyatomic ion" and classifies a competitive shift as a type of kinetic, which "arises from the competitive decay rates between the various fragments".[52]

In the past, PEPICO analyses have used at least one of the two methods or a combination of the two very successfully.[22,28,53−55] In this work, rac-RRKM theory was used for channels where our quantum chemical calculations identified a saddle point on the potential energy surface, *i.e.*, a tight transition state, and SSACM theory was applied for dissociations occurring on a purely attractive potential energy surface. The transitional vibrational frequencies of the transition states (RRKM) or the rigidity factor (SSACM) and the appearance energies were optimized to fit the model to the experimental breakdown diagram and the time-of-flight mass spectra. The latter are a direct measure of the dissociation rates and are used to validate the model dissociation rate curves. In our model, the energy dependent rigidity factor, $f(E)$, for channels modeled by SSACM theory had the following form:

$$f(E) = \exp\left(-\frac{E - E_0}{c_1}\right) + c_2\left[1 - \exp\left(-\frac{E - E_0}{c_1}\right)\right]$$

where $E - E_0$ is the excess energy above the dissociation limit and c_1 and c_2 are adjustable parameters.[49]

RESULTS AND DISCUSSION

Dissociative Photoionization Processes. Threshold PEPICO time-of-flight mass spectra were recorded between 9.5 and 13.8 eV. The dissociative photoionization of methyl vinyl ketone (m/z 70) yields four fragment ions in this photon energy range, namely m/z 55, 43, 42, and 27. With the exception of m/z 42, these fragment ions correspond to the most intense peaks in the EI mass spectrum of methyl vinyl ketone.[56] The low intensity of the m/z 42 fragment ion in the EI mass spectrum can be explained by the fact that its formation proceeds through a tight transition state, and therefore, the other channels outcompete the m/z 42 fragment at energies more than 1 eV above the ionization energy of MVK (*vide infra*). Note, however, that this fragment ion is still present at higher energies, even if its fractional abundance is almost negligible. Based on these m/z peaks, we can establish a preliminary dissociative photoionization mechanism. The m/z 55 fragment ion can only be formed through the loss of a methyl radical from the molecular ion (2). Similarly, there is only one reasonable pathway for the formation of the m/z 43 fragment ion: vinyl radical loss from the molecular ion (3). There are several feasible reactions to yield the other two daughter ions, m/z 42 and 27. The former can be formed directly from the molecular ion through the loss of CO or $CH_2{=}CH_2$. The m/z 42 fragment ion may also be produced by a consecutive H-loss dissociation from the m/z 43 (vinyl-loss) fragment ion. However, this possibility can be excluded based on the breakdown diagram, as the m/z 42 fragment ion has a lower appearance energy than the m/z 43 fragment ion, which, therefore, cannot be its parent ion. Of the two remaining mechanisms for the formation of m/z 42 (CO or $CH_2{=}CH_2$ loss from the molecular ion), one may consider CO-loss to be more likely (1), seeing that it was also reported to be the lowest energy dissociation channel for the structurally similar acrolein molecular ion.[24] Finally, the m/z 27 fragment ion can be the product of an acetyl radical loss directly from the MVK molecular ion (4a), or it can be formed in a consecutive fashion by a CO-loss from the m/z 55 fragment ion through a direct C−C bond cleavage (4b). This is quite similar to the sequential photodissociation of neutral MVK to CH_3, C_2H_3, and CO after photolysis at 193 nm, as reported by Fahr *et al.*[10] Statistical thermodynamics modeling, based on DFT and *ab initio* calculations, was used to identify the dissociative photoionization mechanism unequivocally, and the deduced mechanisms were confirmed and further refined by *ab initio* quantum chemical calculations. These reactions are summarized in eqs 1−4b, ordered by their experimentally derived onsets, going from lowest to highest energy.

https://dx.doi.org/10.1021/acs.jpca.0c10665
J. Phys. Chem. A 2021, 125, 848−856

$$CH_2CHCOCH_3^+ (m/z\ 70) \rightarrow CH_2CHCH_3^+ (m/z\ 42) + CO \quad (1)$$

$$\rightarrow CH_2CHCO^+ (m/z\ 55) + CH_3 \quad (2)$$

$$\rightarrow CH_3CO^+ (m/z\ 43) + CH_2CH \quad (3)$$

$$\rightarrow CH_2CH^+ (m/z\ 27) + CH_3CO \quad (4a)$$

$$CH_2CHCO^+ (m/z\ 55) \rightarrow CH_2CH^+ (m/z\ 27) + CO \quad (4b)$$

The asymmetric fragment ion peaks observed in the time-of-flight spectrum in the 10.2−10.8 eV photon energy range indicate the presence of a metastable molecular ion. As such, the kinetics modeling was carried out by fitting both the experimental breakdown diagram and in this energy range, also the recorded TOF spectra, as shown in Figure 2.

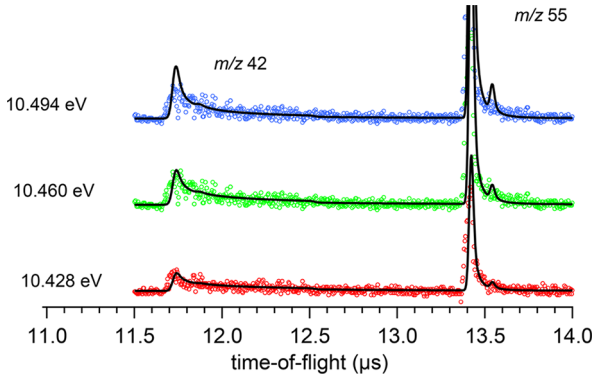

Figure 2. Representative time-of-flight spectra at three different photon energies. Colored circles show the experimental data, whereas solid lines represent the modeled spectra.

Statistical Modeling. Reaction rates and energy distributions were modeled using the tools of statistical thermodynamics and rate theory.[44] In the model, an adiabatic ionization energy (AIE) of 9.66 eV was used, based on our experimentally derived AIE of 9.665 ± 0.013 eV. This value was obtained by fitting the first, most intense peak in the threshold photoelectron spectrum of MVK with a Gaussian function and includes a 0.008 eV redshift due to field ionization in the extraction region.[57] This value is in good agreement with the previous works of Morizur *et al.* (9.66 eV)[58] and Pan *et al.* (9.66 eV),[12] as well as with the G4/W1U calculated values of 9.634/9.680 eV. In the model of the breakdown diagram, a sample temperature of 300 K provided the best fit to the experimental data, consistent with the room temperature effusive inlet source. Appearance energies (E_0's) and either transition state transitional frequencies or rigidity factors of the model were varied to obtain the best fit to the experimental data, as shown in Figure 3. In our final model, the dissociation channel (1) was modeled using RRKM theory, as our quantum chemical calculations identified a tight transition state (saddle point) along the reaction coordinate (*vide infra*), whereas SSACM theory was applied for the remaining four channels, all of which proceed by a loose transition state without a reverse barrier.

The first two fragment ions, m/z 55 and 42, appear approximately at the same photon energy, and the corresponding channels (1) and (2) were optimized simultaneously as parallel dissociations of the MVK molecular ion. The quick rise and fall of m/z 42 (1) indicates that the formation of this species is energetically favored, but it proceeds through a tighter transition state, which is why channel (1) is quickly overtaken by the competing reaction (2), and the fractional abundance of m/z 42 falls to a persistent 2.5−3% above 10.8 eV. The best-fit model provided an experimental E_0 value of 10.48 ± 0.03 eV in reasonable agreement with the calculated 10.530/10.543 eV (G4/W1U) barrier for carbon monoxide loss from the molecular ion (*vide infra*). The m/z 55 fragment ion is formed through a loose transition state, consistent with a direct H_3C-CO bond cleavage, and the experimental appearance energy of 10.55 ± 0.025 eV can be compared with the G4/W1U-calculated thermochemical limit of 10.506/10.545 eV.

Channel (3) produces the m/z 43 fragment ion, most likely by a direct vinyl radical loss from the molecular ion. The best fit of our model provided an experimental appearance energy of 11.01 ± 0.05 eV. This value is almost the exact average of the calculated thermochemical limits of 10.996 and 11.023 eV obtained from G4 and W1U calculations, respectively. As we will show later, this E_0 value is consequential as it serves as the starting point of our thermochemical calculations to derive the heat of formation of the neutral precursor. Therefore, we decided to evaluate how possible systematic errors in the statistical model might affect this value, making sure that SSACM is in fact the right choice for modeling this channel. As

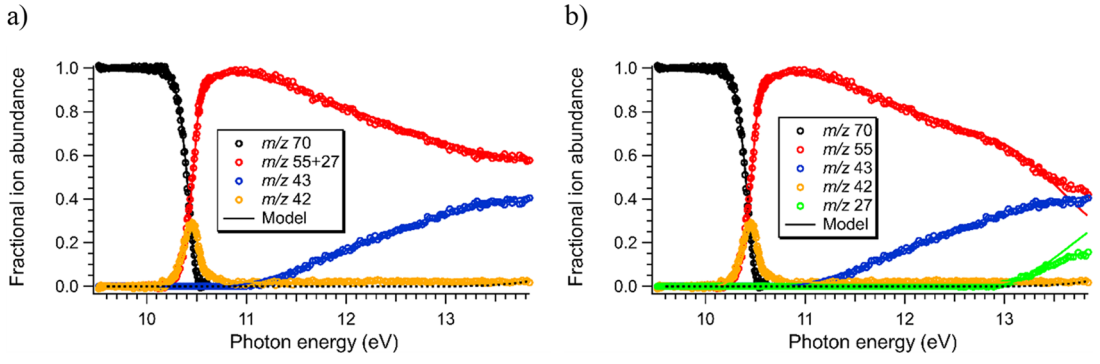

Figure 3. Models of the experimental breakdown diagram. (a) Coincidence signal from the m/z 55 and 27 fragment ions are summed together. (b) Fit of the model after separating the m/z 55 and 27 signal and adding an additional consecutive channel forming the m/z 27 fragment ion. The minor contribution of the parallel m/z 27 channel is depicted as a dashed line in both diagrams.

https://dx.doi.org/10.1021/acs.jpca.0c10665
J. Phys. Chem. A 2021, 125, 848−856

mentioned before, RRKM theory may underestimate the onset of an ionic dissociation occurring on a purely attractive potential energy surface (*i.e.*, reaction without a reverse barrier) when a large kinetic or competitive shift is present.[50] This is indeed the case for (3), which is in competition with (2).

To validate our choice of statistical theories (rac-RRKM for tight and SSACM for loose channels), a second model was constructed in which channels (1−3) were all modeled by (rac-)RRKM theory. Even though this second model resulted in an equally good fit to the experimental data as our original model shown in Figure 3, it did provide a lower E_0 value for channel (3) by more than 0.1 eV (E_0[RRKM] = 10.90 ± 0.05 eV; E_0[SSACM] = 11.01 ± 0.05 eV). Furthermore, the RRKM appearance energy not only deviates more from the G4/W1U calculated thermochemical limits of 10.996/11.023 eV but this second model also predicts the relative difference (ΔE_0) between the onsets of the first two loose channels (2 and 3) to be significantly lower than quantum chemical calculations suggest (ΔE_0[G4/W1U] = 0.490/0.478 eV; ΔE_0[SSACM] = 0.46 ± 0.06 eV; and ΔE_0[RRKM] = 0.37 ± 0.06 eV). We expect that the G4- and W1U-computed appearance energy differences are more reliable than their absolute values, as they are affected by similar errors. Aside from literature evidence,[49] comparing the calculated and modeled appearance energy differences also confirms that the original SSACM model, is in this case, the model of choice to account for the loose channels in this system.

Above 13 eV, the m/z 27 fragment may form either in a parallel fashion, by acetyl radical loss from the parent ion (4a), or in a consecutive CO-loss from the CH_3-loss fragment ion at m/z 55 (4b). As the enthalpies of formation of the possible products of these reactions are all well-known (Table 1), the difference in their appearance energies can be calculated for both proposed mechanisms. In the absence of a reverse barrier, the E_0 difference between two competitive channels is equal to the difference between the heats of formation sum of the ionic and neutral products. Furthermore, in this case, channels (3) and (4a) correspond to a complementary pair of ions/neutrals and the E_0 difference is equal to the difference in the ionization energies of the neutral products: the acetyl and vinyl radicals. Using (3) as a reference, the literature thermochemical data places the appearance energy of the acetyl-loss m/z 27 fragment ion (4a) 1.53 eV higher than that of (3, E_0 = 12.54 eV). However, when the formation of the m/z 27 fragment ion is modeled solely as coming from a direct dissociation (4a) of the parent ion, in parallel with channel (3), the model can only fit the experimental data if the E_0 is lowered below 12.1 eV, indicating that (4a) alone cannot account for all of the experimentally measured m/z 27 signal. Here, we would like to point out an alternative to measuring ionization energies by photoelectron spectroscopy: if the m/z 27 channel from the parent ion was more intense, the vinyl ionization energy, which cannot be measured directly,[26] could nevertheless be established experimentally based on the MVK breakdown diagram, analogously to, *e.g.*, the IE of the isopropyl and the *t*-butyl radicals.[59,60]

Table 1. Known and Derived 0 K Heat of Formation Values Used in this Work

	$\Delta_f H_{0K}$ (kJ mol^{-1})	
species	neutral	cation
CH_3	149.872 ± 0.060[a]	
CO	−113.803 ± 0.026[a]	
CH_2CH	301.13 ± 0.34[a]	1118.94 ± 0.57[a]
CH_3CO	−3.34 ± 0.35[a]	666.41 ± 0.46[a]
CH_2CHCO		<790 ± 10[b];
		773.7 ± 5.4[c]
MVK	−95.65 ± 0.88[a];	838.3 ± 5.4[c]
	−94.3 ± 4.8[c]	

[a]Version 1.122 g of the Active Thermochemical Tables.[67] [b]Li and Baer.[24] [c]This work.

Therefore, the m/z 27 fragment ion is mostly due to a consecutive CH_3 + CO loss mechanism (4b). Does the direct CH_3CO loss (4a) contribute to the m/z 27 peak at all? Using the statistical model, we can address this issue even without explicitly modeling (4b). If the fractional abundance of a secondary fragment ion (produced only through a consecutive dissociation channel) is summed into its precursor ion's abundance, the resulting simplified breakdown diagram can be fit without including the consecutive dissociation. Therefore, to test if channel (4a) also contributes, the experimental breakdown curves of the m/z 27 and 55 fragment ions were summed together and the model, which included only channels (1−3), was fitted to this data (Figure 3a). The best fit of the model indicates that the m/z 27 signal can be accounted for as a sequential product of m/z 55, yet there is a small improvement in the fit if channel (4a) is also included in the mechanism in competition with channels (2) and (3), using the appearance energy of 12.54 eV (*vide supra*), based on the experimental E_0 for m/z 43 and the calculated appearance energy difference of the m/z 43 and 27 channels. While we cannot exclude minor contributions from the parallel channel (4a), the modeling does not conclusively prove that it plays a part in the dissociative photoionization of MVK.

The dominant, consecutive component of the m/z 27 trace was modeled by including (4b) in the statistical model and to make sure that we avoid over-parametrization, with the minor channel (4a) kept frozen in the simulation (Figure 3b). The best fit provided an experimental onset for (4b) at 12.95 eV, which is in agreement with the G4/W1U calculated 12.916/12.961 eV. Channel (4b) is clearly overestimated above 13.3 eV, which we cannot rationalize in the absence of experimental data above 13.8 eV.

To conclude, five dissociation channels reproduce the experimental PEPICO data best: the lowest energy but relatively tight CO-loss (m/z 42, 1), two competing, loose methyl- and vinyl-loss channels (m/z 55 and 43, 2 and 3, respectively), and beyond 12.8 eV, a two-component m/z 27 formation mechanism including both a minor direct CH_3CO and the major consecutive CH_3 + CO dissociation channels (4a) and (4b), respectively. Next, we shall explore the potential energy surface driving the fragmentation processes.

Potential Energy Surface. Reactions confirmed by quantum chemical calculations (see Materials and Methods Section) to play a part in the dissociative photoionization of methyl vinyl ketone are described below and shown in Figure 4. The reported 0 K G4/W1U energies are relative to neutral methyl vinyl ketone.

As mentioned above, the only possibility for the formation of the m/z 55 fragment ion is methyl radical loss from the molecular ion. By scanning the corresponding H_3C−CO bond in the molecular ion, no reverse barrier was found along the methyl-loss reaction coordinate. The calculated thermochem-

https://dx.doi.org/10.1021/acs.jpca.0c10665
J. Phys. Chem. A 2021, 125, 848−856

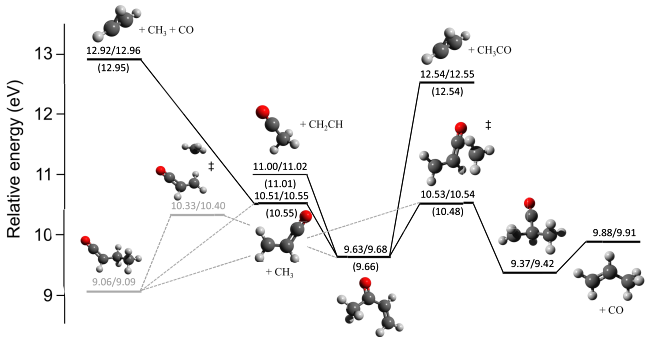

Figure 4. The lowest-energy pathways to each fragment ion in the dissociative photoionization of methyl vinyl ketone. Energies are reported relative to the neutral MVK molecule, calculated using the G4 and W1U methods. Experimentally derived appearance energies from our statistical model are shown in parentheses above which the G4/W1U calculated energies are listed.

ical limits for the formation of the m/z 55 fragment ion and a methyl radical are 10.506/10.545 eV (G4/W1U), in agreement with the experimental value of 10.55 ± 0.025 eV. Similarly, vinyl radical loss from the opposite side of the molecular ion results in the m/z 43 fragment ion and this reaction also proceeds without a reverse barrier. The calculated thermochemical limits of the m/z 43 fragment ion and vinyl radical are 10.996/11.023 eV (G4/W1U level). This is in excellent agreement with 11.01 ± 0.05 eV provided by modeling the breakdown diagram.

As briefly mentioned above, in contrast to the m/z 55 and 43 channels, there are several possible pathways to form the two remaining fragment ions. The m/z 42 daughter ion can be formed from the molecular ion through either CH_2CH_2- or CO-loss. Both of these reactions require prior rearrangement in the parent ion, and thus, both of them proceed through a higher energy transition state structure. This is in good agreement with our experimental finding that even though the appearance energy of the m/z 42 fragment ion is the lowest, this channel is quickly overtaken by the direct methyl- and vinyl-loss dissociations as those both proceed through significantly looser transition states. Ethene-loss from the molecular ion requires a H-shift prior to dissociation and it involves a TS at 11.890/11.892 eV (G4/W1U). Our DFT calculations indicate that the molecular ion dissociates immediately after clearing this barrier and the G4/W1U thermochemical limit is at 10.730/10.767 eV. CO-loss, however, involves a lower-energy intermediate structure at 9.367/9.416 eV, formed by a methyl shift through a transition state at 10.530/10.543 eV (G4/W1U). The methyl-shift intermediate has enough excess energy to immediately form carbon monoxide and ionized propene as the m/z 42 fragment ion. In this transition state, the mobile methyl group gets as far as 2.3 Å from the CH−CO bond, *i.e.*, the rearrangement reaction proceeds for quite far along the methyl-loss reaction coordinate (reaction 2) after which the intramolecular rearrangement takes place. This resembles roaming pathways,[61] except that the methyl migration concludes in isomerization, instead of hydrogen abstraction as in *e.g.*, the isopropanol molecular ion.[18] As this reaction exhibits a low-energy transition state, which agrees well with the experimental E_0 of 10.48 ± 0.03 eV, it most likely represents the correct mechanism for the formation of the m/z 42 fragment ion. While studying the potential energy surface of this methyl hopping, we also located an even lower-lying transition state, at 10.331/10.397 eV (G4/W1U), which leads toward ethyl ketene cation formation. However, the ethyl ketene cation is not only more stable than the methyl vinyl ketone cation but also it shows no distinct fragmentation pathways over MVK at low energies. Therefore, the dissociative photoionization mechanism of MVK and ethyl ketene is shared, and because of the low-lying isomerization transition state, well-merging is likely at the fragmentation thresholds. Moreover, in the absence of well-skipping in the dissociation of the ethyl ketene ion, our statistical model for MVK should be able to describe the ethyl ketene dissociative photoionization accurately as well. Regrettably, as the ethyl ketene DPI has not been recorded yet, the jury is still out whether this proposed mechanism holds true.

As detailed above in the modeling section, the m/z 27 fragment ion can be formed either directly from the molecular ion thorough the loss of acetyl radical or in a consecutive fashion through CH_3- and CO-losses. Scanning along the reaction coordinates for these processes did not reveal reverse barriers in either of these reactions. The calculated appearance energy for the m/z 27 fragment ion is 12.535/12.546 eV in the case of acetyl-radical loss, and 12.916/12.961 eV for consecutive CH_3- and CO-losses (using G4 and W1U methods, respectively), the latter of which agree with the experimental value of 12.95 eV for the CH_3 + CO loss.

Thermochemistry. If a dissociative photoionization reaction does not involve a reverse barrier and the enthalpies of formation are known for all but one species, the unknown value can be calculated using the experimentally derived appearance energy. There is no experimental heat of formation in the recent literature for the neutral MVK, despite its atmospheric relevance. The older values are estimates, based on group additivity rules, or quantum chemical calculations.[31,62−65] Out of these, the most commonly accepted value is reported by Guthrie, based on the hydrogen exchange equilibrium between methyl vinyl ketone and 2-ethyl-2-methyl-1,3-dioxolane in liquid benzene.[31] This 298 K value of −115 ± 11 kJ mol^{-1} can be converted to −99 ± 11 kJ mol^{-1} at 0 K, using the B3LYP/6-311++G(d,p) vibrational frequencies of MVK and the known elemental thermal enthalpies.[66] The most recent 0 K heat of formation value, reported in version 1.122 g of the Active Thermochemical Tables,[67] −95.65 ± 0.88 kJ mol^{-1}, is based on quantum chemical calculations by Ruscic[67] and Durig,[68] and isodesmic reaction enthalpy calculations by Porterfield *et al.*[69] The energetics of the m/z 55 fragment ion, the propenonyl cation, is also unknown. Therefore, the next direct dissociation channel, yielding the acetyl cation at m/z 43, can be used as a starting point for the derivation of thermochemical values. This reaction involves no reverse barrier, and the heats of formation of both of its products are well known. The heat of formation values used in or derived from this work are summarized in Table 1.

From our PEPICO measurements, we can derive the heat of formation of neutral MVK using the experimental appearance energy of the m/z 43 channel. The 0 K gas phase heats of formation of both fragments (vinyl radical: 301.13 ± 0.34 kJ mol^{-1}; acetyl cation: 666.41 ± 0.46 kJ mol^{-1}; see Table 1) are well known. Using these values and our appearance energy of 11.01 ± 0.05 eV, the 0 K heat of formation of MVK is obtained as −94.3 ± 4.8 kJ mol^{-1} (−110.5 ± 4.8 kJ mol^{-1} at 298 K) in good agreement with the calculated −95.65 ± 0.88 kJ mol^{-1} value from ATcT.[67] Combining this value with our MVK AIE

https://dx.doi.org/10.1021/acs.jpca.0c10665
J. Phys. Chem. A 2021, 125, 848−856

of 9.665 ± 0.013 eV, the 0 K heat of formation of the MVK molecular ion can be calculated as 838.3 ± 5.4 kJ mol^{-1}.

Using the heats of formation data determined here, the bond dissociation energy (BDE) between the carbonyl and vinyl groups can be determined in both neutral and ionized methyl vinyl ketone.

$$\mathrm{BDE} = \sum \Delta_f H_{0\mathrm{K}}(\mathrm{fragments}) - \Delta_f H_{0\mathrm{K}}(\mathrm{precursor})$$

In neutral MVK, this bond energy is 392.1 ± 4.8 kJ mol^{-1}, whereas in the molecular ion, it is considerably lower at 129.3 ± 5.4 kJ mol^{-1}. The BDE between the methyl and carbonyl groups in the molecular ion can also be calculated as 85.3 ± 7.6 kJ mol^{-1}, showing that conjugation between the π-orbitals of the vinyl and carbonyl groups represent a stabilizing factor of approximately 40−45 kJ mol^{-1}, compared to the bond between the carbonyl and methyl groups in the molecular ion.

PEPICO spectroscopy has been used before to estimate the 0 K gas phase heat of formation of the CH_2CHCO^+ ion (m/z 55) by Li and Baer.[24] In their work on the dissociative photoionization of acrolein, they determined this value as <790 ± 10 kJ mol^{-1}. They report only an upper limit for the CH_2CHCO^+ ion because of their suspicion that the H-loss channel from the molecular ion of acrolein proceeds through a small reverse barrier. This hypothesis was confirmed by our own quantum chemical calculations (carried out as an auxiliary part of this project), which indicate the involvement of a small reverse barrier in the H-loss dissociation of the acrolein ion. In their work, Li and Baer also questioned the reaction systems and the use of unreliable ancillary data used in previous determinations of the CH_2CHCO^+ heat of formation.[70,71] In the current work, we can determine the 0 K gas phase heat of formation for the CH_2CHCO^+ ion (m/z 55) with greater certainty using the m/z 43 channel as the anchor, which yields 773.7 ± 5.4 kJ mol^{-1}. This value is calculated using the fact that the E_0 difference between channels 2 and 3 corresponds to the difference between the heat of formation sums of their products:

$$\begin{aligned} &E_0(m/z\ 43) - E_0(m/z\ 55) \\ &\quad = [\Delta_f H_{0\mathrm{K}}(CH_3CO^+) + \Delta_f H_{0\mathrm{K}}(CH_2CH)] \\ &\qquad - [\Delta_f H_{0\mathrm{K}}(CH_2CHCO^+) + \Delta_f H_{0\mathrm{K}}(CH_3)] \end{aligned}$$

from which the only unknown value is $\Delta_f H_{0\mathrm{K}}(CH_2CHCO^+)$.

CONCLUSIONS

The dissociative photoionization of methyl vinyl ketone was studied by photoelectron photoion coincidence spectroscopy in the photon energy range of 9.5−13.8 eV. Five major dissociation channels were identified, and their mechanism and energetics were explored by combining quantum chemical calculations with modeling based on statistical thermodynamics. The methyl group was found to be quite mobile, but it does not participate in roaming H-abstraction processes. Instead, below the direct methyl-loss barrier, it can return and bind to either vinyl carbons to form a more stable precursor ion. One of these intermediates is the ethyl ketene cation, and the other leads to CO-loss and the formation of the m/z 42 fragment ion in the lowest-energy DPI channel. The second channel produces the m/z 55 fragment ion through a simple methyl-loss. The third fragment ion (m/z 43) is formed via a vinyl radical loss from the molecular ion of methyl vinyl ketone. Considering the available thermochemical data and our results from modeling the experimental breakdown diagram, it can be deduced that the main source of the m/z 27 fragment ion is a consecutive CO-loss from the methyl-loss fragment ion, m/z 55. The m/z 27 fragment ion may also be formed via a direct acetyl radical loss from the molecular ion. Although the onset of this parallel channel is lower than that of consecutive one, it only has a small contribution (less than ∼3%) to the overall relative abundance of the fragment ion because of competition with other parallel channels with significantly lower onsets.

Based on our experimental data, the first directly measured, experimentally derived 0 K heat of formation of methyl vinyl ketone is reported here as −94.3 ± 4.8 kJ mol^{-1}. Using B3LYP vibrational frequencies of MVK and the known elemental thermal enthalpies, this value can be converted to −110.5 ± 4.8 kJ mol^{-1} at 298 K. We also propose a new, experimentally derived 0 K gas phase heat of formation value for one of the main fragments of the dissociative photoionization of MVK, the $C_2H_3CO^+$ (m/z 55) ion at 773.7 ± 5.4 kJ mol^{-1}. This value improves the accuracy of previously available ones by approximately a factor of two, and provides an exact value instead of an upper limit.[24] As this ion is also formed in the dissociation of other small oxygenated molecules, this value can be used to determine further thermochemical properties of these systems or to improve the existing values.

AUTHOR INFORMATION

Corresponding Author

Bálint Sztáray − *Department of Chemistry, University of the Pacific, Stockton, California 95211, United States;* orcid.org/0000-0002-0333-0000; Email: bsztaray@pacific.edu

Authors

Peter Weidner − *Department of Chemistry, University of the Pacific, Stockton, California 95211, United States;* orcid.org/0000-0003-1261-3886

Amelia W. Ray − *Department of Chemistry, University of the Pacific, Stockton, California 95211, United States;* orcid.org/0000-0002-4350-9371

Andras Bodi − *Laboratory for Synchrotron Radiation and Femtochemistry, Paul Scherrer Institute, Villigen 5232, Switzerland;* orcid.org/0000-0003-2742-1051

Complete contact information is available at: https://pubs.acs.org/10.1021/acs.jpca.0c10665

Notes

The authors declare no competing financial interest.

ACKNOWLEDGMENTS

This work was funded by the National Science Foundation (grant no. CHE-1665464). Experiments were performed at the VUV beamline of the Swiss Light Source at the Paul Scherrer Institute. This manuscript has been submitted on the 42nd birthday of Dr. A.B. and his co-authors wish to extend their congratulations on this occasion.

REFERENCES

(1) Wang, K.-Y.; Shallcross, D. E. Modelling terrestrial biogenic isoprene fluxes and their potential impact on global chemical species using a coupled LSM−CTM model. *Atmos. Environ.* **2000**, *34*, 2909−2925.

(2) Müller, J.-F.; Stavrakou, T.; Wallens, S.; De Smedt, I.; Van Roozendael, M.; Potosnak, M. J.; Rinne, J.; Munger, B.; Goldstein, A.; Guenther, A. B. Global isoprene emissions estimated using MEGAN, ECMWF analyses and a detailed canopy environment model. *Atmos. Chem. Phys.* **2008**, *8*, 1329−1341.
(3) Guenther, A. B.; Jiang, X.; Heald, C. L.; Sakulyanontvittaya, T.; Duhl, T.; Emmons, L. K.; Wang, X. The Model of Emissions of Gases and Aerosols from Nature version 2.1 (MEGAN2.1): an extended and updated framework for modeling biogenic emissions. *Geosci. Model Dev.* **2012**, *5*, 1471−1492.
(4) Peeters, J.; Nguyen, T. L.; Vereecken, L. HO_x radical regeneration in the oxidation of isoprene. *Phys. Chem. Chem. Phys.* **2009**, *11*, 5935−5939.
(5) Lelieveld, J.; Butler, T. M.; Crowley, J. N.; Dillon, T. J.; Fischer, H.; Ganzeveld, L.; Harder, H.; Lawrence, M. G.; Martinez, M.; Taraborrelli, D.; et al. Atmospheric oxidation capacity sustained by a tropical forest. *Nature* **2008**, *452*, 737−740.
(6) Atkinson, R. Atmospheric chemistry of VOCs and NO_x. *Atmos. Environ.* **2000**, *34*, 2063−2101.
(7) Wennberg, P. O.; Bates, K. H.; Crounse, J. D.; Dodson, L. G.; McVay, R. C.; Mertens, L. A.; Nguyen, T. B.; Praske, E.; Schwantes, R. H.; Smarte, M. D.; et al. Gas-phase reactions of isoprene and its major oxidation products. *Chem. Rev.* **2018**, *118*, 3337−3390.
(8) Fan, J.; Zhang, R. Atmospheric oxidation mechanism of isoprene. *Environ. Chem.* **2004**, *1*, 140−149.
(9) Earle, M. E.; Mills, R.; Roscoe, J. M. The photolysis of methyl vinyl ketone at 308nm. *J. Photochem. Photobiol., A* **2009**, *206*, 71−79.
(10) Fahr, A.; Braun, W.; Laufer, A. H. Photolysis of methyl vinyl ketone at 193.3 nm: quantum yield determinations of methyl and vinyl radicals. *J. Phys. Chem.* **1993**, *97*, 1502−1506.
(11) Romero, M. T. B.; Blitz, M. A.; Heard, D. E.; Pilling, M. J.; Price, B.; Seakins, P. W.; Wang, L. Photolysis of methylethyl, diethyl and methylvinyl ketones and their role in the atmospheric HO_x budget. *Faraday Discuss.* **2005**, *130*, 73−88.
(12) Pan, G.; Hu, C.; Huang, M.; Wang, Z.; Cheng, Y.; Liu, Z.; Gu, X.; Zhao, W.; Zhang, W.; Chen, J.; et al. A VUV photoionization mass spectrometric study on the OH-initiated photooxidation of isoprene with synchrotron radiation. *J. Environ. Sci.* **2012**, *24*, 2075−2082.
(13) Gierczak, T.; Burkholder, J. B.; Talukdar, R. K.; Mellouki, A.; Barone, S. B.; Ravishankara, A. R. Atmospheric fate of methyl vinyl ketone and methacrolein. *J. Photochem. Photobiol., A* **1997**, *110*, 1−10.
(14) Praske, E.; Crounse, J. D.; Bates, K. H.; Kurtén, T.; Kjaergaard, H. G.; Wennberg, P. O. Atmospheric fate of methyl vinyl ketone: Peroxy radical reactions with NO and HO_2. *J. Phys. Chem. A* **2014**, *119*, 4562−4572.
(15) Fogleman, E. A.; Koizumi, H.; Kercher, J. P.; Sztáray, B.; Baer, T. Heats of formation of the acetyl radical and ion obtained by threshold photoelectron photoion coincidence. *J. Phys. Chem. A* **2004**, *108*, 5288−5294.
(16) Stockbauer, R. A threshold photoelectron−photoion coincidence mass spectrometer for measuring ion kinetic energy release on fragmentation. *Int. J. Mass Spectrom. Ion Phys.* **1977**, *25*, 89−101.
(17) Rennie, E. E.; Boulanger, A.-M.; Mayer, P. M.; Holland, D. M.; Shaw, D. A.; Cooper, L.; Shpinkova, L. G. A photoelectron and TPEPICO investigation of the acetone radical cation. *J. Phys. Chem. A* **2006**, *110*, 8663−8675.
(18) Covert, K. J.; Bodi, A.; Torma, K. G.; Voronova, K.; Baer, T.; Sztáray, B. To roam or not to Roam, That is the question for the methyl group in isopropanol cations. *Int. J. Mass Spectrom.* **2021**, *459*, 116469.
(19) Covert, K. J.; Voronova, K.; Torma, K. G.; Bodi, A.; Zádor, J.; Sztáray, B. Thermochemistry of the smallest QOOH radical from the roaming fragmentation of energy selected methyl hydroperoxide ions. *Phys. Chem. Chem. Phys.* **2018**, *20*, 21085−21094.
(20) Bodi, A.; Baer, T.; Wells, N. K.; Fakhoury, D.; Klecyngier, D.; Kercher, J. P. Controlling tunnelling in methane loss from acetone ions by deuteration. *Phys. Chem. Chem. Phys.* **2015**, *17*, 28505−28509.
(21) Bodi, A.; Hemberger, P.; Gerber, T. A robust link between the thermochemistry of urea and isocyanic acid by dissociative photoionization. *J. Chem. Thermodyn.* **2013**, *58*, 292−299.
(22) Bodi, A.; Hemberger, P. Low-Energy Photoelectron Spectrum and Dissociative Photoionization of the Smallest Amides: Formamide and Acetamide. *J. Phys. Chem. A* **2018**, *123*, 272−283.
(23) Kercher, J. P.; Fogleman, E. A.; Koizumi, H.; Sztáray, B.; Baer, T. Heats of formation of the propionyl ion and radical and 2,3-pentanedione by threshold photoelectron photoion coincidence spectroscopy. *J. Phys. Chem. A* **2005**, *109*, 939−946.
(24) Li, Y.; Baer, T. The dissociation dynamics and thermochemistry of the acrolein ion studied by threshold photoelectron−photoion coincidence spectroscopy. *Int. J. Mass Spectrom.* **2002**, *218*, 37−48.
(25) Tang, X.; Gu, X.; Lin, X.; Zhang, W.; Garcia, G. A.; Fittschen, C.; Loison, J.-C.; Voronova, K.; Sztáray, B.; Nahon, L. Vacuum ultraviolet photodynamics of the methyl peroxy radical studied by double imaging photoelectron photoion coincidences. *J. Chem. Phys.* **2020**, *152*, 104301.
(26) Wu, X.; Zhou, X.; Hemberger, P.; Bodi, A. The ionization energy of the vinyl radical: a Mexican standoff with a happy ending. *Phys. Chem. Chem. Phys.* **2019**, *21*, 22238−22247.
(27) Torma, K. G.; Voronova, K.; Sztáray, B.; Bodi, A. Dissociative Photoionization of the C_7H_8 Isomers Cycloheptatriene and Toluene: Looking at Two Sides of the Same Coin Simultaneously. *J. Phys. Chem. A* **2019**, *123*, 3454−3463.
(28) Voronova, K.; Torma, K. G.; Kercher, J. P.; Bodi, A.; Sztáray, B. Dissociative photoionization of chromium hexacarbonyl: A round-trip ticket to non-statisticality and a detective story in thermochemistry. *Int. J. Mass Spectrom.* **2019**, *438*, 63−71.
(29) Voronova, K.; Mozaffari Easter, C. M.; Covert, K. J.; Bodi, A.; Hemberger, P.; Sztáray, B. Dissociative photoionization of diethyl ether. *J. Phys. Chem. A* **2015**, *119*, 10654−10663.
(30) Bodi, A.; Csontos, J.; Kállay, M.; Borkar, S.; Sztáray, B. On the protonation of water. *Chem. Sci.* **2014**, *5*, 3057−3063.
(31) Guthrie, J. P. Equilibrium constants for a series of simple aldol condensations, and linear free energy relations with other carbonyl addition reactions. *Can. J. Chem.* **1978**, *56*, 962−973.
(32) Johnson, M.; Bodi, A.; Schulz, L.; Gerber, T. Vacuum ultraviolet beamline at the Swiss Light Source for chemical dynamics studies. *Nucl. Instrum. Methods Phys. Res., A* **2009**, *610*, 597−603.
(33) Sztáray, B.; Voronova, K.; Torma, K. G.; Covert, K. J.; Bodi, A.; Hemberger, P.; Gerber, T.; Osborn, D. L. CRF-PEPICO: Double velocity map imaging photoelectron photoion coincidence spectroscopy for reaction kinetics studies. *J. Chem. Phys.* **2017**, *147*, No. 013944.
(34) Bodi, A.; Sztáray, B.; Baer, T.; Johnson, M.; Gerber, T. Data acquisition schemes for continuous two-particle time-of-flight coincidence experiments. *Rev. Sci. Instrum.* **2007**, *78*, No. 084102.
(35) Eppink, A. T. J. B.; Parker, D. H. Velocity map imaging of ions and electrons using electrostatic lenses: Application in photoelectron and photofragment ion imaging of molecular oxygen. *Rev. Sci. Instrum.* **1997**, *68*, 3477−3484.
(36) Wiley, W. C.; McLaren, I. H. Time-of-flight mass spectrometer with improved resolution. *Rev. Sci. Instrum.* **1955**, *26*, 1150−1157.
(37) Frisch, M.; Trucks, G.; Schlegel, H.; Scuseria, G.; Robb, M.; Cheeseman, J.; Scalmani, G.; Barone, V.; Mennucci, B.; Petersson, G.; et al. *Gaussian 09*, revision A. 2; Gaussian, Inc.: Wallingford, CT, 2009.
(38) Becke, A. D. A new mixing of Hartree−Fock and local density-functional theories. *J. Phys. Chem.* **1993**, *98*, 1372−1377.
(39) Lee, C.; Yang, W.; Parr, R. G. Development of the Colle-Salvetti correlation-energy formula into a functional of the electron density. *Phys. Rev. B* **1988**, *37*, 785.
(40) Fukui, K. The path of chemical reactions - the IRC approach. *Acc. Chem. Res.* **1981**, *14*, 363−368.
(41) Curtiss, L. A.; Redfern, P. C.; Raghavachari, K. Gaussian-4 theory. *J. Chem. Phys.* **2007**, *126*, No. 084108.

https://dx.doi.org/10.1021/acs.jpca.0c10665
J. Phys. Chem. A 2021, 125, 848−856

(42) Martin, J. M. L.; de Oliveira, G. Towards standard methods for benchmark quality *ab initio* thermochemistry—W1 and W2 theory. *J. Chem. Phys.* **1999**, *111*, 1843—1856.
(43) Parthiban, S.; Martin, J. M. L. Assessment of W1 and W2 theories for the computation of electron affinities, ionization potentials, heats of formation, and proton affinities. *J. Chem. Phys.* **2001**, *114*, 6014—6029.
(44) Sztáray, B.; Bodi, A.; Baer, T. Modeling unimolecular reactions in photoelectron photoion coincidence experiments. *J. Mass Spectrom.* **2010**, *45*, 1233—1245.
(45) Rice, O. K.; Ramsperger, H. C. Theories of unimolecular gas reactions at low pressures. *J. Am. Chem. Soc.* **1927**, *49*, 1617—1629.
(46) Rice, O. K.; Ramsperger, H. C. Theories of unimolecular gas reactions at low pressures. II. *J. Am. Chem. Soc.* **1928**, *50*, 617—620.
(47) Marcus, R. A.; Rice, O. K. The Kinetics of the Recombination of Methyl Radicals and Iodine Atoms. *J. Phys. Chem.* **1951**, *55*, 894—908.
(48) Beyer, T.; Swinehart, D. F. Algorithm 448: number of multiply-restricted partitions. *Commun. ACM* **1973**, *16*, 379.
(49) Troe, J.; Ushakov, V. G.; Viggiano, A. A. On the model dependence of kinetic shifts in unimolecular reactions: the dissociation of the cations of benzene and *n*-butylbenzene. *J. Phys. Chem. A* **2006**, *110*, 1491—1499.
(50) Stevens, W.; Sztáray, B.; Shuman, N.; Baer, T.; Troe, J. Specific rate constants $k(E)$ of the dissociation of the halobenzene ions: analysis by statistical unimolecular rate theories. *J. Phys. Chem. A* **2009**, *113*, 573—582.
(51) Chupka, W. A. Effect of unimolecular decay kinetics on the interpretation of appearance potentials. *J. Phys. Chem.* **1959**, *30*, 191—211.
(52) Lifshitz, C. Time-resolved appearance energies, breakdown graphs, and mass spectra: The elusive "kinetic shift". *Mass Spectrom. Rev.* **1982**, *1*, 309—348.
(53) Russell, E. M.; Cudjoe, E.; Mastromatteo, M. E.; Kercher, J. P.; Sztáray, B.; Bodi, A. From Iron Pentacarbonyl to the Iron Ion by Imaging Photoelectron Photoion Coincidence. *J. Phys. Chem. A* **2013**, *117*, 4556—4563.
(54) Rowland, T. G.; Sztáray, B.; Armentrout, P. B. Metal—Cyclopentadienyl Bond Energies in Metallocene Cations Measured Using Threshold Collision-Induced Dissociation Mass Spectrometry. *J. Phys. Chem. A* **2013**, *117*, 1299—1309.
(55) Bodi, A.; Sigurdardottir, K. L.; Kvaran, Á.; Bjornsson, R.; Arnason, I. Dissociative Photoionization of 1-Halogenated Silacyclohexanes: Silicon Traps the Halogen. *J. Phys. Chem. A* **2016**, *120*, 9188—9197.
(56) NIST Mass Spectrometry Data Center, William E. Wallace, director, *"Mass Spectra", in NIST Chemistry WebBook, NIST Standard Reference Database Number 69*, Eds. P.J. Linstrom and W.G. Mallard, National Institute of Standards and Technology, Gaithersburg MD, 20899, https://doi.org/10.18434/T4D303, (retrieved March 30, 2020).
(57) Bodi, A.; Shuman, N. S.; Baer, T. On the ionization and dissociative photoionization of iodomethane: a definitive experimental enthalpy of formation of CH_3I. *Phys. Chem. Chem. Phys.* **2009**, *11*, 11013—11021.
(58) Morizur, J.-P.; Mercier, J.; Sarraf, M. 2-substituted-2,3-dihydro-4*H*-pyrans: Competition between 'retro Diels-Alder'fragmentation and substituent loss. *Org. Mass Spectrom.* **1982**, *17*, 327—330.
(59) Stevens, W. R.; Bodi, A.; Baer, T. Dissociation Dynamics of Energy Selected, Propane, and i-$C_3H_7X^+$ Ions by iPEPICO: Accurate Heats of Formation of i-$C_3H_7^+$, i-C_3H_7Cl, i-C_3H_7Br, and i-C_3H_7I. *J. Phys. Chem. A* **2010**, *114*, 11285—11291.
(60) Stevens, W. R.; Walker, S. H.; Shuman, N. S.; Baer, T. Dissociative photoionization study of neopentane: a path to an accurate heat of formation of the *t*-butyl ion, *t*-butyl iodide, and t-butyl hydroperoxide. *J. Phys. Chem. A* **2010**, *114*, 804—810.
(61) Joalland, B.; Shi, Y.; Kamasah, A.; Suits, A. G.; Mebel, A. M. Roaming dynamics in radical addition—elimination reactions. *Nat. Commun.* **2014**, *5*, 4064.
(62) Dellon, L. D.; Sung, C.-Y.; Robichaud, D. J.; Broadbelt, L. J. Group Additivity Determination for Oxygenates, Oxonium Ions, and Oxygen-Containing Carbenium Ions. *Ind. Eng. Chem. Res.* **2017**, *56*, 10259—10270.
(63) Kondo, S.; Takahashi, A.; Tokuhashi, K. Theoretical calculation of heat of formation and heat of combustion for several flammable gases. *J. Hazard. Mater.* **2002**, *94*, 37—45.
(64) Benson, S. W.; Cruickshank, F. R.; Golden, D. M.; Haugen, G. R.; O'Neal, H. E.; Rodgers, A. S.; Shaw, R.; Walsh, R. Additivity rules for the estimation of thermochemical properties. *Chem. Rev.* **1969**, *69*, 279—324.
(65) Benson, S. W.; Buss, J. H. Additivity rules for the estimation of molecular properties. Thermodynamic properties. *J. Phys. Chem.* **1958**, *29*, 546—572.
(66) Wagman, D. D.; Evans, W. H.; Parker, V. B.; Schumm, R. H.; Halow, I. *The NBS tables of chemical thermodynamic properties. Selected values for inorganic and C1 and C2 organic substances in SI units*; National Standard Reference Data System: 1982.
(67) Ruscic, B.; Bross, D. H. *Active Thermochemical Tables (ATcT) values based on ver. 1.122g of the Thermochemical Network (2019)*. ATcT.anl.gov (accessed 2020).
(68) Durig, J. R.; Little, T. S. Conformational barriers to internal rotation and vibrational assignment of methyl vinyl ketone. *J. Phys. Chem.* **1981**, *75*, 3660—3668.
(69) Porterfield, J. P.; Nguyen, T. L.; Baraban, J. H.; Buckingham, G. T.; Troy, T. P.; Kostko, O.; Ahmed, M.; Stanton, J. F.; Daily, J. W.; Ellison, G. B. Isomerization and fragmentation of cyclohexanone in a heated micro-reactor. *J. Phys. Chem. A* **2015**, *119*, 12635—12647.
(70) Holmes, J. L.; Terlouw, J. K.; Burgers, P. C. $[C_3H_3O]^+$ ions; reacting and non-reacting configurations. *Org. Mass Spectrom.* **1980**, *15*, 140—143.
(71) Traeger, J. C.; Hudson, C. E.; McAdoo, D. J. The distonic ion·$CH_2CH_2CO^+$ and its formation from ionized cyclopentanone. *Org. Mass Spectrom.* **1989**, *24*, 230—234.

NOTE ADDED AFTER ISSUE PUBLICATION

This paper was published January 19, 2021. It was not noted for inclusion in the Cheuk-Yiu Ng Festschrift virtual special issue. The note was added and the paper was reposted on February 1, 2021.

https://dx.doi.org/10.1021/acs.jpca.0c10665
J. Phys. Chem. A 2021, 125, 848—856